Angewandte Chemie International Edition

10.1002/anie.202424037

RESEARCH ARTICLE

Dendritic Platinum Nanoparticles Shielded by Pt-S PEGylation as Intracellular Reactors for Bioorthogonal Uncaging Chemistry

Jose I. Garcia-Peiro,[a,b,c,d],± M. Carmen Ortega-Liebana,[e,f,g,h],±,* Catherine Adam,[e],± Álvaro Lorente-Macías,[e] Jana Travnickova,[e,i] E. Elizabeth Patton,[e,i] Paula Guerrero-López,[h,j] J. Manuel Garcia-Aznar,[h,j] Jose L. Hueso,[a,b,c,d,k],* Jesus Santamaria[a,b,c,d],* and Asier Unciti-Broceta[e],*

[a] Instituto de Nanociencia y Materiales de Aragon (INMA), CSIC-Universidad de Zaragoza, Edificio I+D, C/ Poeta Mariano Esquillor s/n, 50018 Zaragoza, Spain.

[b] Department of Chemical and Environmental Engineering, University of Zaragoza, Campus Rio Ebro, C/ María de Luna, 3, 50018 Zaragoza, Spain.

[c] Networking Research Center in Biomaterials, Bioengineering and Nanomedicine (CIBER-BBN), Instituto de Salud Carlos III, 28029 Madrid, Spain.

[d] Instituto de Investigación Sanitaria (IIS) de Aragón, Avenida San Juan Bosco, 13, 50009 Zaragoza, Spain.

[e] Edinburgh Cancer Research, Cancer Research UK Scotland Centre, Institute of Genetics and Cancer, University of Edinburgh, Crewe Road South, Edinburgh EH4 2XR, UK.

[f] Department of Medicinal and Organic Chemistry and Unit of Excellence in Chemistry Applied to Biomedicine and Environment, Faculty of Pharmacy, Campus Cartuja s/n, University of Granada, 18071 Granada, Spain.

[g] GENYO, Pfizer/University of Granada/Andalusian Regional Government, PTS Granada, Avda. Ilustración 114, 18016 Granada, Spain.

[h] Instituto de Investigación Biosanitaria ibs.GRANADA, Granada, Spain.

[i] MRC Human Genetics Unit, Institute of Genetics and Cancer, University of Edinburgh, Crewe Road South, Edinburgh EH4 2XR, UK.

[j] Multiscale in Mechanical and Biological Engineering (M2BE), Aragon Institute of Engineering Research (I3A), University of Zaragoza, Mariano Esquillor s/n, 50018 Zaragoza, Spain

[k] Escuela Politécnica Superior, Universidad de Zaragoza. Crta. de Cuarte s/n, 22071, Huesca, Spain.

± Equal contribution

*Emails: asier.ub@ed.ac.uk; jesus.santamaria@unizar.es; jlhueso@unizar.es; mcortega@ugr.es

Supporting information for this article is given via a link at the end of the document.

Abstract: *Beyond their classical role as cytotoxics, Platinum (Pt) coordination complexes recently joined the selected group of transition metals capable of performing bioorthogonal reactions in living environments. To minimize their reactivity towards nucleophiles, which limit their catalytic performance, we investigated the use of Pt(0) with different forms, sizes and surface functionalization. We report herein the development of PEGylated Pt nanodendrites with the capacity to activate prodyes and prodrugs in cell culture and in vivo. Their dendritic morphology together with their surface shielding through Pt-S-bonded PEGylation synergistically contributed to create catalytic nanoreactors compatible with the highly-crowded and reductive environment of the cell cytoplasm, thereby facilitating in situ bioorthogonal drug uncaging in cancer cells in 2D and 3D culture, including in microfluidic systems, and xenografted in zebrafish.*

Introduction

A myriad of bioorthogonal reactions and targeting strategies have been combined over a decade to unleash the pharmacological effects of drugs on demand at desired anatomical locations.[1] The "chemistries" used to release these bioactive agents range from purely organic methods (e.g., click-to-release strategies)[2] to physicochemical (e.g., photo- or ultrasound-induced bond-cleavage)[3] and organometallic reactions (e.g., uncaging reactions mediated by Pd or Ru).[4] While differing in the nature of the stimulus that triggers the activation process, all these strategies share the goal of maximizing drug efficacy and attenuating toxicity by the on-site release of therapeutics (e.g., inside a tumor).

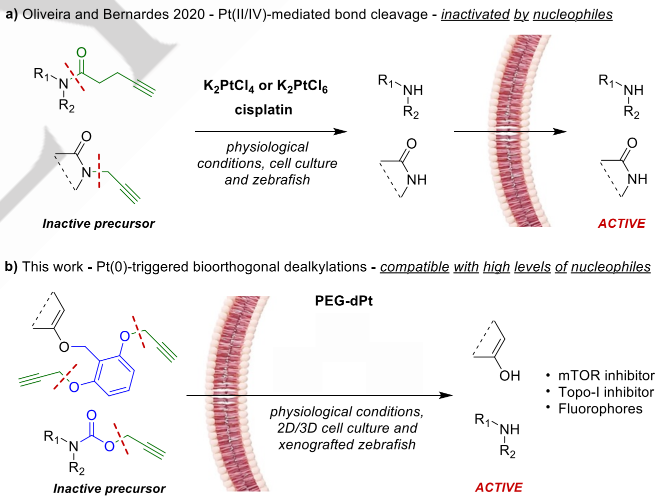

Scheme 1. a, Pt(II/IV)-mediated bioorthogonal bond cleavage reported by Oliveira and Bernardes.[12a] The reactivity of the Pt(II/IV) complexes towards cell nucleophiles restricts their performance inside cells. **b**, Pt(0)-catalyzed uncaging strategy developed in this work. Nanodendrite protection with PEG-SH enhanced the bioorthogonal chemistry capabilities of metallic Pt inside cells.

Pd,[5] Ru,[6] Au,[7] Fe[8] and Cu[9] have been extensively studied for the uncaging of prodrugs or for the local assembly of active drugs from inactive precursors. These metals are typically used in free form (e.g., discrete organometallic complexes or nanoparticles) or coordinated / embedded into vesicles and polymeric materials. So far, the most successful strategies *in vivo* have relied on catalytic devices that release drugs in the interstitial space,[10] since the stringent conditions of the intracellular environment severely reduce the efficacy of most metal catalysts.[11]

10.1002/anie.202424037

Other transition metals such as Pt have recently entered the toolbox of abiotic catalysts that can mediate bioorthogonal reactions in biological environments.[12] Oliveira and Bernardes[12a] demonstrated that Pt(II/IV) complexes —including the anticancer drug cisplatin— can mediate bond-cleavage reactions under physiological conditions; specifically, the uncaging of pentynoyl tertiary amides and *N*-propargyl groups (**Scheme 1a**). The reactivity of Pt complexes towards these groups was exploited to uncage masked precursors of the cytotoxic agents monomethyl auristatin E and 5-fluorouracil in cell culture and in zebrafish, respectively. Later, Huang[12b] developed an inactive Pt(IV) complex conjugated to an O^2-propargyl diazeniumdiolate moiety. Upon reduction of Pt(IV) to Pt(II) inside cells, cisplatin is released to both attack the cells and mediate *O*-depropargylation and release of nitric oxide. These seminal works showcase the potential of homogeneous Pt catalysis, particularly with a divalent oxidation state, in prodrug activation. However, the electrophilic reactivity of these complexes towards glutathione and other intracellular nucleophiles is shown to decrease their capacity to mediate uncaging reactions by 6−15 fold in cell culture.[12a] Moreover, the inherent genotoxicity of Pt coordination species (cisplatin, oxaliplatin and carboplatin are DNA crosslinking agents widely used in the clinic as standard chemotherapy)[13] limit their use as truly bioorthogonal (= biologically inert) catalysts.

With minimal inherent toxicity and featuring unique redox, photothermal (PT) and metallic properties, heterogeneous Pt(0)-based nanomaterials can drive the decomposition of H_2O_2, induce PT cell ablation upon UV-to-NIR irradiation or interact with external electric fields to mediate charge polarization, leading to hole-doping conditions able to transform water molecules into reactive oxygen species.[14] Another advantage of Pt(0) is its straightforward synthesis from oxidized Pt species using green reagents such as ascorbic acid and the possibility of assembly into dendritic nanoparticles (dPt) with high surface area.[15] Interestingly, despite these features, the potential capacity and use of Pt(0) to mediate bioorthogonal uncaging reactions in complex environments has not yet been investigated. We rationalized that tuning the structure and surface composition of Pt nanoparticles (NPs), including size, surface area-to-volume ratio and stabilizing ligands, could enable us to find the optimum set of features required to achieve bioorthogonal reactivity, while maintaining the excellent stability, biocompatibility and biodistribution profile of this class of nanodevices.

Following the above strategy, herein we demonstrate a bioorthogonal catalytic role for Pt(0) (**Scheme 1b**). We also explored the most suitable Pt(0)-mediated uncaging reaction by developing ten different masking groups with two different dyes. Optimization of nanocatalyst reactivity and compatibility with nucleophiles was achieved by PEG shielding through Pt-S functionalization. The best performing prodye + PEGylated dPt combination demonstrated high catalytic properties under physiologically relevant conditions and inside cancer cells implanted in zebrafish. Finally, the bioorthogonal applicability of Pt(0) in complex environments was challenged and validated by the *in situ* activation of two prodrugs of the anticancer agents SN-38 (topoisomerase I inhibitor) and sapanisertib (mTOR kinase inhibitor) in cell culture, in cancer spheroids in a microfluidic system and *in vivo*.

Results and Discussion

Synthesis and characterization of Pt NPs. H_2PtCl_6 (metal source) and ascorbic acid (reductive agent) were used to prepare a range of Pt NPs using different synthetic protocols (**Figure 1a**). Preliminary experiments demonstrated that Pt(0) nanostructures with spherical dimensions performed poorly as uncaging catalysts and, therefore, our efforts focused on the development of NPs with dendritic form. Polymer-assisted synthesis was performed by adding H_2PtCl_6 plus the surfactant PVP (MW 40,000) (**dPt-1**) or Pluronic F-127 (**dPt-2**) in deionized H_2O at room temperature (r. t.), followed by addition of ascorbic acid. The resulting suspension was kept overnight at 37 ºC. Unreacted precursors and byproducts were discarded by two centrifugation cycles. We also prepared uncoated Pt NPs by changing the ratio of reagents and heating up the reaction to 90 ºC for 10 min (**dPt-3**). Afterwards, the unreacted precursors and byproducts were discarded by centrifugation (x2, 10 min, r. t.) (see full protocol in the Supp. Info.). Encouragingly, TEM and HAADF-STEM imaging showed that the three Pt NPs featured a dendritic shape (**Figure 1b**, and **Figure S1a-c**, Supp. Info.), which is an optimal feature to maximize the surface area-to-volume ratio, thereby increasing the number of active centers available for reaction. **Figure 1b** shows representative TEM images of the dendritic shape and the size analysis of each NP type (by ImageJ), showing average diameters moderately increasing from 40 to 60 nm from **dPt-1** to **dPt-3**. Measurements of the Zeta potential (ZP) revealed that all the nanodendrites were characterized by negative charge surface: -22 mV for **dPt-1**, -24 mV for **dPt-2** and -16 mV for **dPt-3** (**Figure 1b**).

The NPs were further characterized using X-ray diffraction (XRD) and X-ray photoelectron spectroscopy (XPS). XRD analysis clearly showed patterns that perfectly correlate with those of the Pt(0) cubic structure[15c] (**Figure 1d**). XPS analysis corroborated the presence of Pt in the nanostructure (**Tables S1-S2**, see Supporting Information). None of the samples presented Pt species in a tetravalent oxidation state, demonstrating the successful reduction of the Pt(IV) precursor, whereas Pt(II) was present in all the nanoparticles at different ratios (**Table S1**, Supp. Inf.). As shown in the table, the nanodendrites synthesized with PVP (**dPt-1**) or Pluronic F-127 (**dPt-2**) presented a superior proportion of Pt(0) than Pt(II) at the external layers of the NPs. Interestingly, these two types of NPs featured different levels of Pt content, with **dPt-2** having approximately 10% higher proportion of Pt content (**Table S2**, Supp. Inf.). The uncoated **dPt-3** displayed the highest proportion of Pt element of all NPs and 100 % of Pt(II) species at the external layers of the NPs, which suggests that the lack of a polymeric material protecting the surface of the NPs exposes the metal to environmental oxidation.

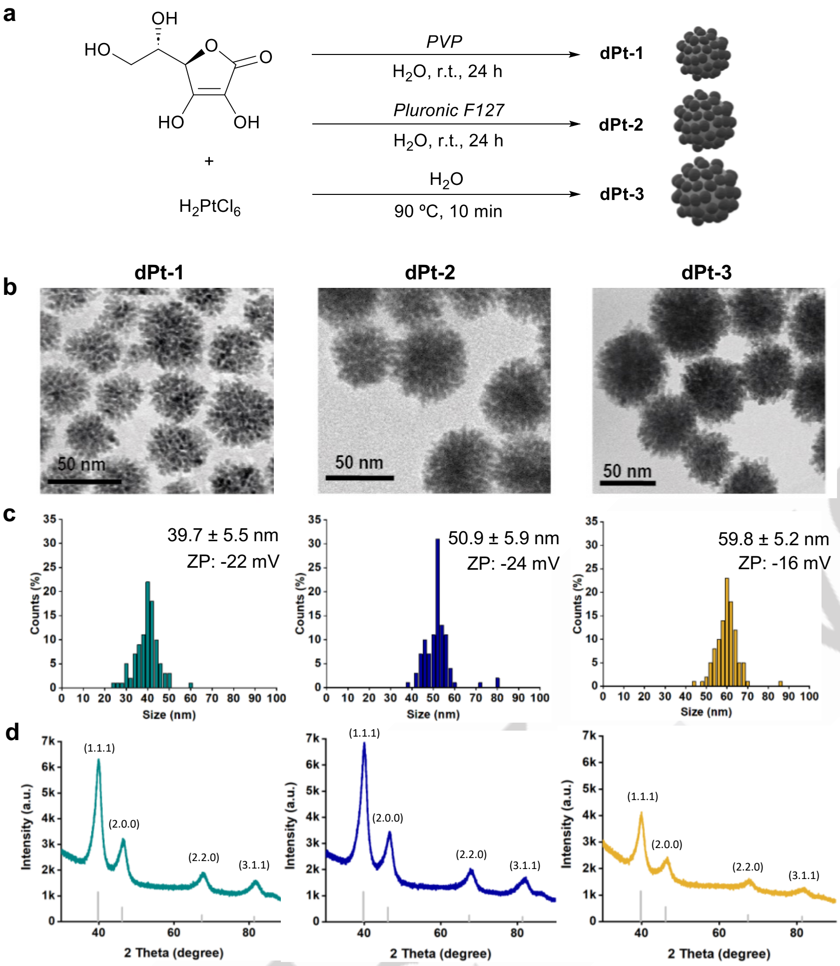

Figure 1. **a**, Synthesis of Pt nanodendrites **dPt-1**, **dPt-2** and **dPt-3**. **b**, TEM images of representative Pt NPs showing a dendritic shape. **c**, Size distribution and zeta potential of **dPt-1**, **dPt-2** and **dPt-3**. Moderate differences in size were observed between the different synthetic protocols. **d**, X-ray diffractograms corresponding to Pt NPs synthetized under each different protocol. XRD analysis displayed patterns that correspond to the cubic structure of Pt.

Design, synthesis and screening of 10-member library of masked prodyes. To assess the uncaging capabilities of the Pt-NPs, we prepared a library of prodyes designed to test the Pt(0)-mediated uncaging of five functional groups: ethers, esters, carbonates, amides and carbamates (**Figure 2a**). Resorufin (Em= 584 nm) was used for the synthesis of the *O*-allyl and *O*-propargyl derivatives **1a** and **1b**, pentenoyl and pentynoyl esters **2a** and **2b**, and allyl and propargyl carbonates **3a** and **3b**. Green-fluorescent EtNH-NBD (Em= 536 nm) was used to prepare pentenoyl and pentynoyl amides **4a** and **4b**, and the allyl and propargyl-oxycarbonyl derivatives **5a** and **5b**. Synthesis protocols are fully described in the Supporting Information. Spectroscopic analysis demonstrated that the fluorescent properties of each of prodyes were quenched by the masking group, with a reduction of fluorescence emission superior to 100-fold (**Figure S2**, Supp. Inf.).

The capabilities of each of the NPs (40 µg/mL, approx. 40 µM in Pt content) to convert the custom-designed library of optically silenced prodyes (40 µM) into active dyes was first tested in PBS at 37 °C. After 24 h, fluorescence intensity was measured with a microplate reader (Ex/Em= 550/580 nm for resorufin; Ex/Em= 485/535 nm for EtNH-NBD) and conversion efficiency calculated by normalizing to the emission of the corresponding dye (= 100%).

From the resorufin-based prodyes (**Figure 2b**), only the allyl ether **1a** was minimally uncaged by Pt(0), with **dPt-2** displaying slightly superior uncaging properties. From the NBD-based prodyes (**Figure 2c**), the alkyne-containing prodyes **4b** and **5b** showed the highest reactivity in the presence of Pt NPs, where **dPt-2** once again exhibiting slightly superior uncaging properties.

Before analyzing the compatibility of the catalysts to more complex media, we measured the stability of the library in PBS supplemented with 10 % serum (rich in esterases) or S9 fraction (which contains both phase I and phase II metabolic enzymes). The study showed that esters **2a,b** and carbonates **3a,b** display very low stability under these conditions and thus were discarded from the following studies (**Figure S3**, Supp. Inf.). Although the rest of the prodyes were stable in the presence of serum and S9 fraction, **5b** was found to be the most stable of the library.

Next, the reaction of each of the Pt NPs with the six remaining prodyes was re-tested in serum-supplemented media. As shown in **Figure 2d**, the catalytic properties of the NPs were significantly reduced in the presence of serum proteins. The best performing nanocatalyst was once again **dPt-2** (synthesized with the assistance of Pluronic F-127). The higher Pt content of **dPt-2** might play a role in its superior catalytic properties.

10.1002/anie.202424037

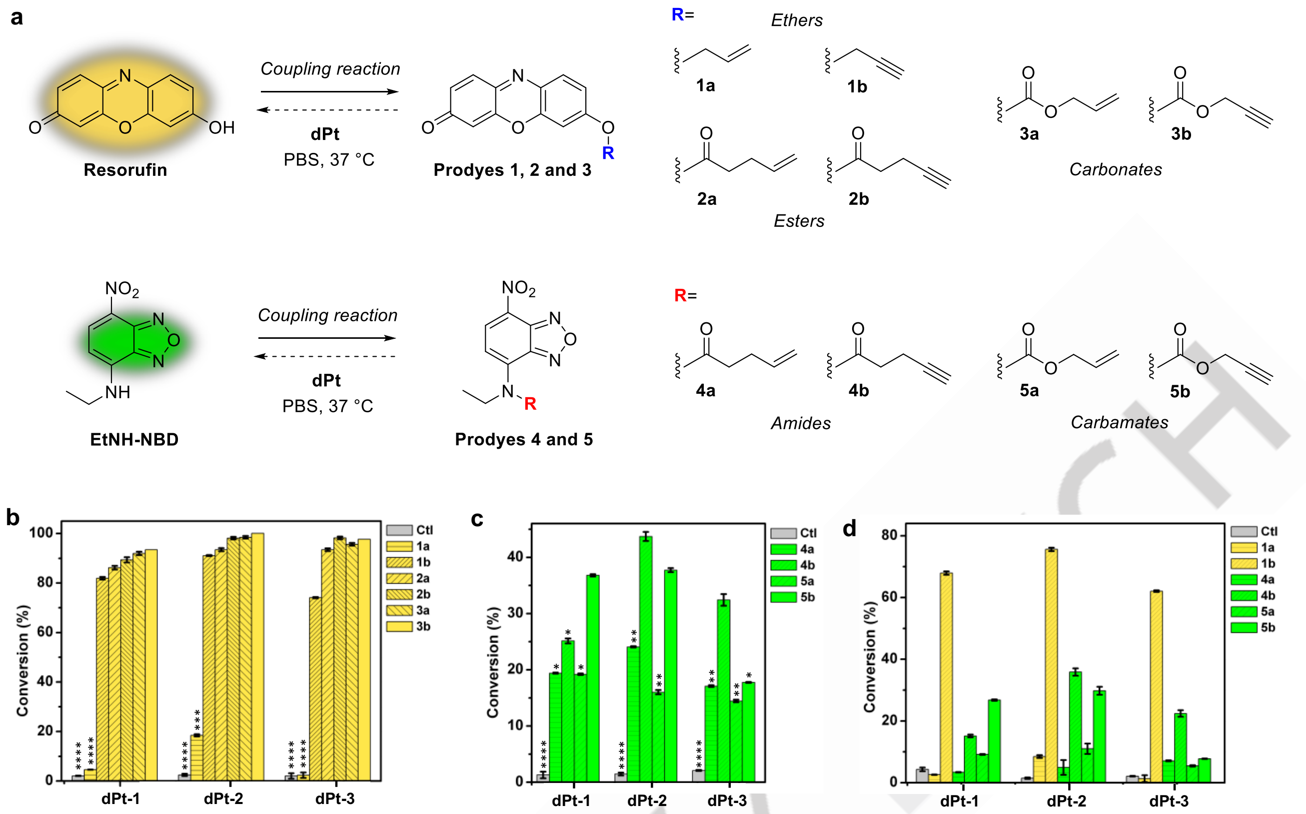

Figure 2. **a**, Synthesis of prodyes **1-5a,b** and Pt-mediated conversion into **resorufin** and **EtNH-NBD**. **b**,**c**, Comparative study of the conversion efficiencies (in %) after 24 h incubation. Reaction conditions: prodye (40 µM) and **dPt-1-3** (40 µg/mL) in PBS at 37 °C. Error bars: ± SD (n = 3). Significant differences relative to the highest conversion value are represented as *P ≤ 0.05, **P ≤ 0.01, ***P ≤ 0.001, ****P ≤ 0.0001. **d,** Comparative study of the conversion efficiencies (in %) after 24 h incubation in PBS supplemented with serum (10% FBS). Negative control (Ctl): prodye without nanocatalysts. Error bars: ± SD (n = 3).

From the range of prodyes with adequate metabolic stability, the compounds featuring a triple bond were the most sensitive to Pt(0) chemistry, highlighting prodye **1b**. Although **5b** was not as efficiently activated as **1b**, it was the most stable prodye to serum and S9 fraction, making it a good candidate for *in vivo* studies. It is also worth noting that the pentynoyl protected prodye **4b** was cleaved with similar efficacy than **5b**. Despite the promising results, a slight reduction of uncaging efficacy was observed for **dPt-2** in the presence of serum, which motivated us to further improve the catalytic capacity of the nanodevices.

Surface functionalization and biocompatibility study. Pluronic F-127-templated **dPt-2** was chosen for subsequent studies based on the fluorogenic uncaging studies. Since they showed slightly reduced catalytic activity in the presence of serum, we devised a strategy to diminish the biofouling effect of proteins and peptides on the nanoparticle surface. Yang and coworkers have recently showed that the Pt-S bond is highly stable and superior to Au-S bond in protecting from cleavage by biogenic thiols.[16] Inspired by this work, following the synthesis and purification protocol **dPt-2** above described, the resulting nanodendrites were further treated with polyethylene glycol methyl ether thiol (PEG-SH, MW=2,000) for 30 min in PBS at r. t. (**Figure 3a**). Unreacted PEG-SH was discarded by two centrifugation cycles of 10 min in water to generate **PEG-dPt-2**. Characterization revealed a slight increase in size (71.7 nm) and drop in zeta potential (-18 mV) without changes in morphology (**Figure S1d,e**, Supp. Inf).

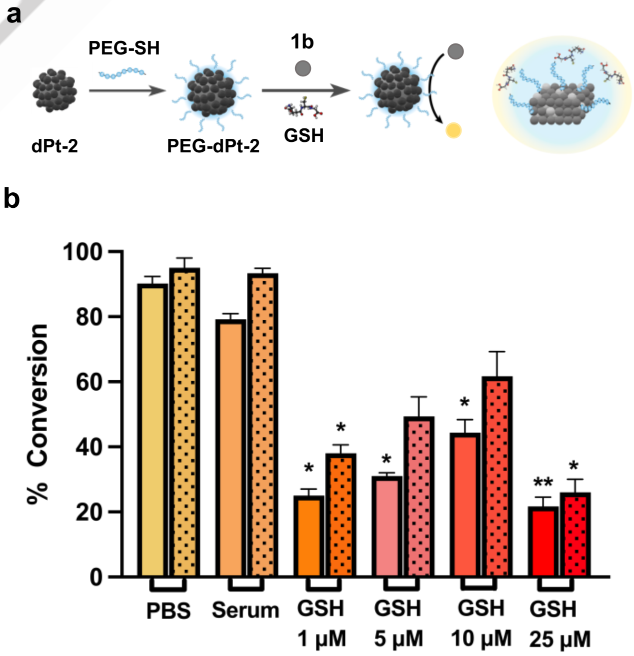

Figure 3. **a**, Synthesis of **PEG-dPt-2**. **b**, Study of the influence of serum and glutathione (GSH) on the fluorogenic reaction of prodye **1b** (40 µM) and **dPt-2** (plain bars) or **PEG-dPt2** (dotted bars) at 80 µg/mL for 24 h. PBS: control without additives (serum or GSH). Error bars: ± SD from n = 3. Significant differences relative to control are represented as *P ≤ 0.05, **P ≤ 0.01.

10.1002/anie.202424037

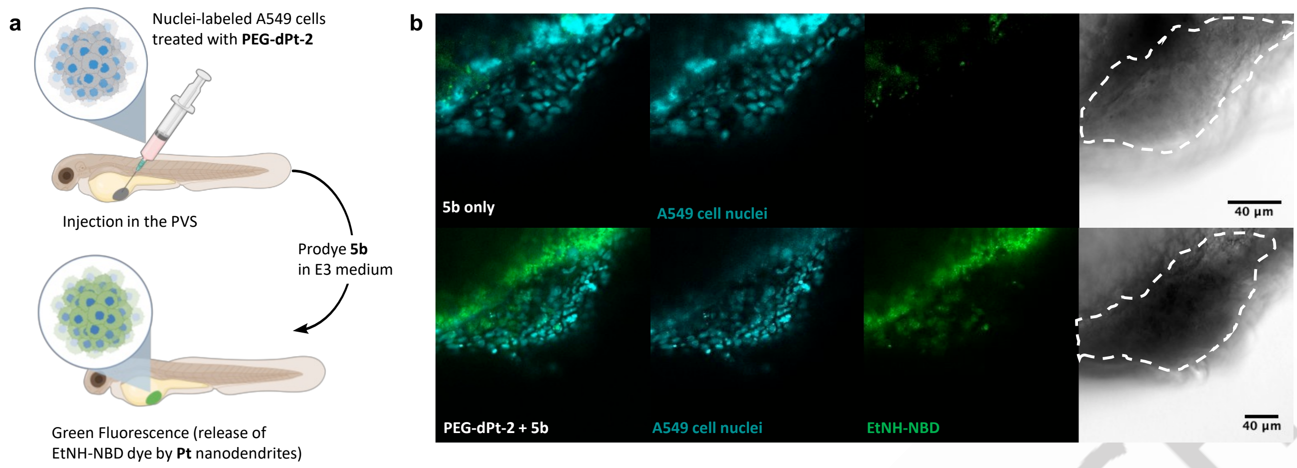

Figure 4. a, Pt(0)-mediated prodye uncaging *in vivo* (created with BioRender). **b**, Confocal analysis of **EtNH-NBD** generation (green) from non-fluorescent **5b** in nuclei-labeled A549 cells (cyan) implanted into the PVS of 2-dpf zebrafish larvae: top, cells without NPs; bottom, cells with loaded with **PEG-dPt-2**. Embryos were imaged two days after injection. N=6. Scale bars = 40 µm.

Probe **1b** was used to evaluate the catalytic properties of **dPt-2** and **PEG-dPt-2** in the presence of serum and glutathione (GSH). Encouragingly, the catalytic properties of **PEG-dPt-2** were not affected by the presence of serum. In addition, the PEGylated nanodendrites tolerated the presence of GSH better than **dPt-2** (**Figure 3b**). Although very high GSH levels (0.5-10 mM) further decreased the catalytic properties of Pt NPs, competition with serum proteins significantly reduced the detrimental effects of GSH (**Figure S4**, Supp. Inf.).

To confirm the catalytic behavior of Pt(0), a recyclability study consisting of performing eight successive reaction cycles with **1b** and **PEG-dPt-2** in the absence and presence of serum was performed (**Figure S5**, Supp. Inf.). Notably, the nanodevices performed well under both conditions, supporting their functional suitability for complex environment. Cell viability assays with A549 cells confirmed that the devices did not induce cytotoxicity up to 0.2 mg/mL (**Figure S6**, Supp. Inf.).

Pt(0)-mediated prodye activation *in vivo*. Motivated by the catalytic compatibility of **PEG-dPt-2** in complex media and the tolerability of cells to Pt(0) treatment, we next challenged the functionality of the NPs *in vivo* in a xenografted zebrafish model (see **Figure 4a**). A549 cells were pre-incubated with the **PEG-dPt-2** for 4 h, to enable NPs internalization, and Hoescht 33342, to fluorescently label cell nuclei. A549 only treated with Hoescht 33342 were used as negative control. Treated cells were then injected in the perivitelline space (PVS) of zebrafish embryos two days post-fertilization (dpf). Zebrafish with successfully implanted **PEG-dPt-2**-treated cells were randomly distributed into two groups (n=6), and treated with E3 media only (non-probe control) or media containing probe **5b** at 2.5 µM in E3 media (fluorogenic experiment) for 40 h. As non-Pt control, zebrafish implanted with nuclei-labeled cells without NPs were treated probe **5b** (2.5 µM) for 40 h. Next, embryos were anaesthetized with tricaine and embedded in 1% (w/v) low melting point agarose (in E3 media) for confocal microscopy imaging and analysis. As shown in the top panel of **Figure 4b**, the control group (no Pt NPs) treated with **5b** exhibited minimal background green fluorescence. Equivalent results were observed in embryos containing **PEG-dPt-2**-treated cells in the absence of **5b** (see **Figure S7**, Supp. Inf.). Notably, the **PEG-dPt-2**-treated group incubated with **5b** showed significant increase in fluorescence emission in the PVS of the embryos, demonstrating the localized generation of **EtNH-NBD**.

Pt(0)-mediated prodrug activation in 2D and 3D cell culture. After demonstrating the capacity of Pt NPs to uncage fluorogenic probes *in vitro* and *in vivo*, we next tested the capabilities of Pt(0) to activate prodrugs in cancer cell culture. Experiments were performed in cancer cell lines with two masked prodrugs: **pro-SN38**, a prodrug of the Topoisomerase I inhibitor SN38 (active metabolite of irinotecan) that has been shown to be effectively activated by Palladium,[17] and novel prodrug **Poc-INK128**, generated by Poc-functionalization of the primary amino group of the benzoxazole moiety of the mTOR inhibitor sapanisertib (a.k.a. INK128). The employ of each of these prodrugs was inspired on the most successful Pt(0)-sensitive masking strategies found from the screening of the prodye library, specifically **1b** (for **pro-SN38**) and **5b** (for **pro-INK128**).

Based on the clinical use of irinotecan in colorectal cancer,[18] HCT116 cells was the model used to test the in situ activation of **pro-SN38** by Pt(0) NPs (**Figure 5a**). To evaluate the efficacy of the PEGylation strategy, **dPt-2** and **PEG-dPt-2** were tested at a range of concentrations (20, 40 and 80 µg/mL). Cells were incubated with the NPs for 3 h, followed by prodrug addition (10, 30 and 100 nM in media supplemented with serum). **SN38** at the same concentration range was used as positive control, while treatment with only Pt or **pro-SN38** were used as negative controls. Cell viability was measured using the PrestoBlue reagent after five days. As shown in **Figure 5** (see experiments with 20 and 40 µg/mL in **Figure S8**, Supp. Inf.), on their own, Pt(0) NPs were well tolerated by HCT116 cells, and the prodrug showed no or minimal antiproliferative effect at the three concentrations used. In contrast, the combined treatment of Pt(0) and prodrug led to equivalent antiproliferative effect as cytotoxic **SN38**. Of note, **PEG-dPt-2** + prodrug consistently induced higher cell death levels, versus experiments with **dPt-2**, confirming the enhancing effect of Pt-S PEGylation on intracellular catalysis.

10.1002/anie.202424037

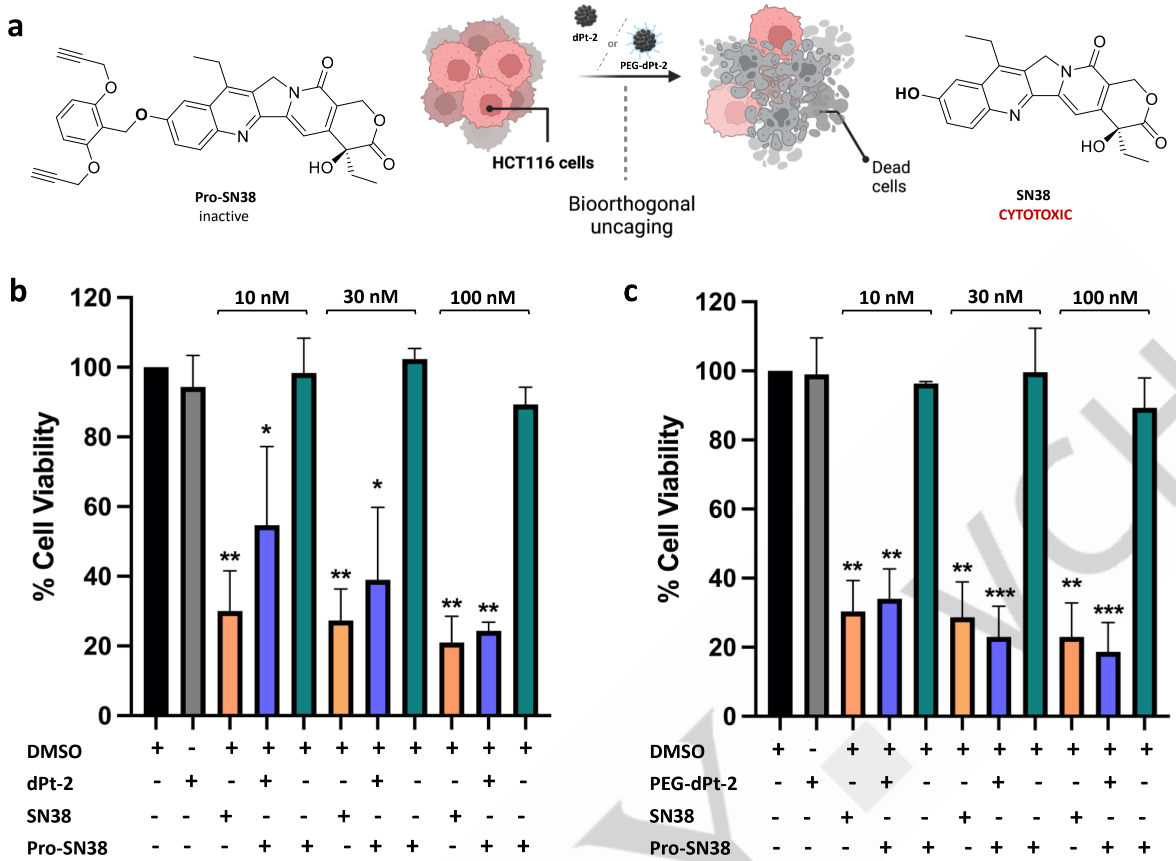

Figure 5. a, Pt-mediated conversion of prodrug **Pro-SN38** into cytotoxic SN38 (created with BioRender). **b,** Cell viability assay in HCT116 colon carcinoma cells under different treatment conditions using **dPt-2**. **c,** Cell viability assay in HCT116 colon carcinoma cells under different treatment conditions using **PEG-dPt-2**. [Prodrug/drug]= 10-30-100 nM. Cells were treated with **dPt-2** (80 µg/mL) or **PEG-dPt-2** (80 µg/mL) followed by the prodrug. PrestoBlue viability assay was performed 5 days after treatment. Error bars: ±SEM, n=3. Significant differences relative to DMSO control are represented as *P ≤ 0.05, **P ≤ 0.01, ***P ≤ 0.001.

Lung adenocarcinoma A549 cells were used to test the Pt(0)-mediated activation of **pro-INK128**, since sapanisertib received fast tracked designation to treat non-small cell lung carcinoma.[19] As shown in **Figure S9** (Supp. Inf.), the dose response curves of **pro-INK128** and sapanisertib showed a significant reduction of antiproliferative activity for the masked drug, providing sufficient therapeutic window to test the *in situ* activation of **pro-INK128** in A549 cells pre-labeled with Pt(0) NPs. Next, prodrug activation experiments were performed as above described. Results shown in **Figure S10** (Supp. Inf.) further corroborated the superior capacity of **PEG-dPt-2** to uncage prodrug in cell culture and generating toxic effects equivalent to the direct treatment with sapanisertib. The prodrug activation experiment (**PEG-dPt-2** + **pro-INK128**) was further validated in 3D culture using A549 spheroids (see **Figure S11**, Supp. Inf.). We evaluated spheroid growth in microchips treated with **pro-INK128** and the **PEG-dPt-2** NPs. After 4 days, control spheroids grew significantly, whereas those treated with **pro-INK128** and the **PEG-dPt-2** remained inhibited (**Figure S12**, Supp. Inf.). Statistical analysis confirmed significant differences in spheroid size distributions across treatments, demonstrating the efficacy of **PEG-dPt-2** to activate **pro-INK128** (**Figure S13**, Supp. Inf.).

Pt(0)-mediated prodrug activation in vivo. Zebrafish embryos provide a rapid, versatile and amenable-to-imaging *in vivo* platform to discriminate differential anticancer therapy responses with single-cell resolution.[20] This model is particularly useful for the initial screening of novel bioorthogonal strategies,[5a,7b,d,12a] for which the ethical justification required to use adult animals is difficult to argue due to the preliminary nature of the studies. Consequently, to evaluate the efficacy of Pt(0) to activate an anticancer agent *in vivo*, we employed a xenograft zebrafish embryo model.

First, we tested the potential toxicity of **pro-SN38** to zebrafish. The tolerability study showed that embryos' viability and development was unaltered after 3 days of incubation with the prodrug at 30 nM, concentration that was selected for the subsequent studies. Following an analogous protocol to the one used for the probe activation studies (**Figure 6a**), HCT116 cells were pre-incubated with **PEG-dPt-2** for 4 h, fluorescently stained with Hoechst 33342 for nuclei labeling and injected into the PVS of 2-dpf zebrafish larvae. Cells labelled only with Hoechst 33342 (no Pt(0)) were used as negative control. At 2 h post injection, embryos were randomly distributed into the different groups and treated: **pro-SN38**, **PEG-dPt-2** and **PEG-dPt-2** + **pro-SN38**. Xenografted fish with no treatment were used as control to normalize tumor growth.

10.1002/anie.202424037

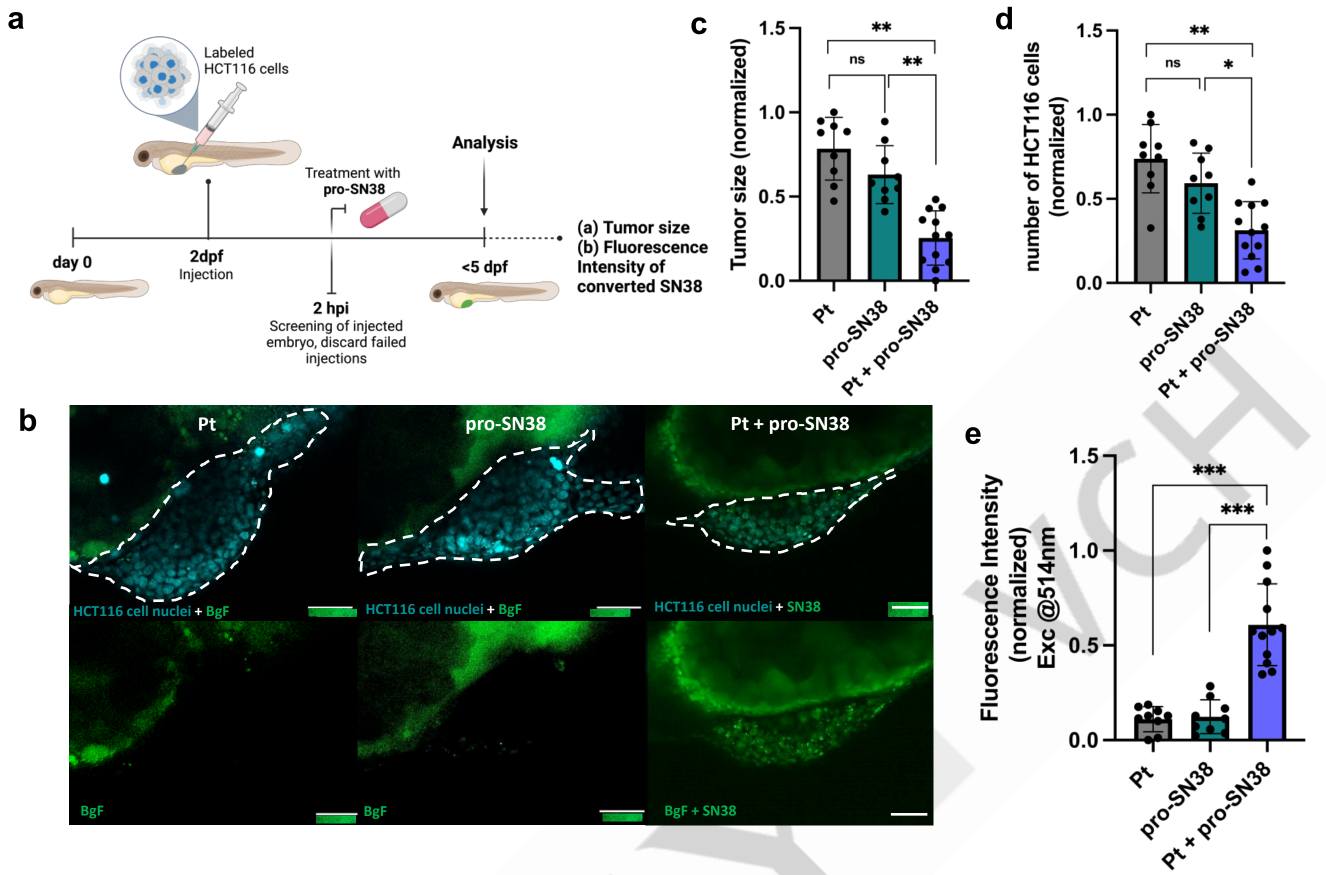

Figure 6. **a**, Schematic timeline of the Pt(0)-mediated prodrug activation *in vivo* assay (created with BioRender). dpf: days post-fertilization; hpi: hours post-injection. **b**, Confocal microscopy images of nuclei-labeled HCT116 cells (cyan) implanted in the PVS of 2-dpf zebrafish larvae after 2 days of incubation in E3 medium with or without **pro-SN38**. Groups: non-Pt-treated cells + **pro-SN38** (left); **PEG-dPt-2**-treated cells + DMSO (middle), and **PEG-dPt-2**-treated cells + **pro-SN38** (left). N= 9-12. The dashed line represents the tumor area. Scale bars = 50 µm. BgF: Background fluorescence. **c**, Measurement of tumor size between groups after treatment. **d**, Analysis of the number of nuclei-labeled cancer cells between groups after treatment. **e,** Quantitative analysis of green fluorescence signal (Ex= 514 nm). Statistical analysis: one-way ANOVA followed by Tukey's post-hoc test: ns >0.05, *P ≤ 0.05, **P ≤ 0.01, ***P ≤ 0.001.

Zebrafish xenografts were imaged by confocal microscopy 2 days after the start of the treatment (**Figure 6b**). Zebrafish treated separately with either **PEG-dPt-2** or **pro-SN38** did not lead to significant changes in tumor size. In contrast, imaging analysis (by ImageJ) of embryos xenografted with **PEG-dPt-2** treated cancer cells and treated **pro-SN38** showed significant reduction ($P \leq 0.01$) of tumor growth (**Figure 6c**) and cancer cell numbers (**Figure 6d**).

Since the active drug **SN38** is fluorescent and, unlike **pro-SN38**, can be excited at 514 nm,[17] we also analyzed green fluorescence emission from the xenografts by confocal microscopy. As shown in **Figure 6b** and analyzed in **Figure 6d**, strong fluorescence emission was only observed from the cancer cells treated with both **PEG-dPt-2** and **pro-SN38**, confirming the *in situ* generation of SN38. Notably, green fluorescence emission colocalized with that of Hoechst 33342-labeled cell nuclei, indicating that the active drug is bound to its target, the nuclear protein Topoisomerase I. The results of the zebrafish assays not only demonstrate the capacity of Pt(0) to generate an anticancer drug *in vivo*, but also served as a target engagement study.

Conclusion

The results presented in this manuscript support the admission of Pt into the selected group of metallic NPs —until now formed by Pd and Au— with the capacity to mediate depropargylation reactions in a true bioorthogonal manner. It also shows the potential of Pt-S functionalization for protecting the catalytic performance of Pt NPs. This study expands the reach of noble metal-based nanodevices in bioorthogonal catalysis and offers new opportunities to modulate the optical properties and bioactivity of small molecules in the highly crowded intracellular environment.

Supporting Information

The authors have cited additional references within the Supporting Information.

Acknowledgements

We are grateful to the EC (H2020-MSCA–IF–2018-841990) and EPSRC (EP/S010289/1) for financial support. We also would like to acknowledge the European Research Council (ERC) through the Catalytic Dual-Function Devices Against Cancer (CADENCE-742684) project, RLDI/2015-021. EEP is funded by the MRC (MC_UU_00035/13), Melanoma Research Alliance and Rosetrees Trust (MRA Awards 687306, 917226). This work was supported by the Cancer Research UK Scotland Centre (CTRQQR-2021\100006). MCOL is grateful to the Institute of Genetics and Cancer (IGC) for financial support through the Hastie Career Advancement Fund 2020, and the Consejeria de Universidad Investigacion e Innovacion by ERDF Andalusian Program 2021-2027 (A-EXP-278-UGR23). We thank IGC Zebrafish facility for supporting zebrafish management and IGC Imaging Facility for their support with imaging experiments. P.G-L. gratefully acknowledges the support of the Government of Aragon (Grant No 2021-25). The synthesis of materials has been performed by the Platform of Production of Biomaterials and Nanoparticles of the NANBIOSIS ICTS, more specifically by the Nanoparticle Synthesis Unit of the CIBER in BioEngineering, Biomaterials & Nanomedicine (CIBER-BBN). The TEM studies were conducted at the Laboratorio de Microscopias Avanzadas, Instituto de Nanociencia y Materiales de Aragon, Universidad de Zaragoza, Spain. (SAI and ELECMI). Ayuda CEX2023-001286-S financiada por MICIU/AEI /10.13039/501100011033.

Keywords: bioorthogonal • catalysis • platinum • heterogeneous • anticancer drugs

[1] a) S. L. Scinto, D. A. Bilodeau, R. Hincapie, W. Lee, S. S. Nguyen, M. Xu, C. W. am Ende, M. G. Finn, K. Lang, Q. Lin, J. P. Pezacki, J. A. Prescher, M. S. Robillard, J. M. Fox. *Nat. Rev. Methods Primers* **2021**, 1, 30; b) W. Wang, X. Zhang, R. Huang, C.-M. Hirschbiegel, H. Wang, Y. Ding, V. M. Rotello, *Adv. Drug Delivery Rev.* **2021**, *176*, 113893; c) Sabatino, V. B. Unnikrishnan, G. J. L. Bernardes, *Chem Catal.* **2022**, *2*, 39-51.

[2] X. Ji, Z. Pan, B. Yu, L. K. De La Cruz, Y. Zheng, B. Ke, B. Wang, *Chem. Soc. Rev.* **2019**, 48, 1077-1094.

[3] Q. Fu, S. Shen, P. Sun, Z. Gu, Y. Bai, X. Wanga, Z. Liu, *Chem. Soc. Rev.* **2023**, 52, 7737-7772.

[4] M. O. N. van de L'Isle, M. C. Ortega-Liebana, A. Unciti-Broceta, *Curr. Opin. Chem. Biol.* **2021**, *61*, 32-42.

[5] a) J. T. Weiss, J. C. Dawson, K. G. Macleod, W. Rybski, C. Fraser, C. Torres-Sanchez, E. E. Patton, M. Bradley, N. O. Carragher, A. Unciti-Broceta, *Nat. Commun.* **2014**, *5*, 3277; b) G. Y. Tonga, Y. D. Jeong, B. Duncan, T. Mizuhara, R. Mout, R. Das, S. T. Kim, Y. C. Yeh, B. Yan, S. Hou, V. M. Rotello, *Nat. Chem.* **2015**, *7*, 597-603; c) B. Rubio-Ruiz, J. T. Weiss, A. Unciti-Broceta, *J. Med. Chem.* **2016**, *59*, 9974-9980; d) T. L. Bray, M. Salji, A. Brombin, A. M. Perez-Lopez, B. Rubio-Ruiz, L. C. A. Galbraith, E. E. Patton, H. Y. Leung, A. Unciti-Broceta, *Chem. Sci.* **2018**, *9*, 7354-7361; e) F. Wang, Y. Zhang, Z. Du, J. Ren, X. Qu, *Nat. Commun.* **2018**, *9*, 1209; f) B. J. Stenton, B. L. Oliveira, M. J. Matos, L. Sinatra, G. J. L. Bernardes, *Chem. Sci.* **2018**, *9*, 4185; g) M. Sancho-Albero, B. Rubio-Ruiz, A. M. Perez-Lopez, V. Sebastian, P. Martin-Duque, M. Arruebo, J. Santamaria, A. Unciti-Broceta, *Nature Catalysis* **2019**, *2*, 864-872; h) A. M. Perez-Lopez, B. Rubio-Ruiz, T. Valero, R. Contreras-Montoya, L. A. de Cienfuegos, V. Sebastian, J. Santamaria, A. Unciti-Broceta, *J. Med. Chem.* **2020**, *63*, 9650-9659; i) J. Lee, S. Dubbu, N. Kumari, A. Kumar, J. Lim, S. Kim, I. S. Lee, *Nano Letters* **2020**, *20*, 6981-6988; j) M. A. Plunk, A. Alaniz, O. P. Olademehin, T. L. Ellington, K. L. Shuford, R. R. Kane, *ACS Med. Chem. Lett.* **2020**, *11*, 141-146; k) R. Das, J. Hardie, B. P. Joshi, X. Zhang, A. Gupta, D. C. Luther, S. Fedeli, M. E. Farkas, V. M. Rotello, *JACS Au* **2022**, *2*, 1679-1685; l) Y. Zhang, L. Zhang, W. Wang, Q. Deng, M. Liu, Z. Zhu, H. Liu, J. Ren, X. Qu, *Angew. Chemie Int. Ed.* **2023**, *62*, e202306395; m) E. Nestoros, F. de Moliner, F. Nadal-Bufi, D. Seah, M. C. Ortega-Liebana, Z. Cheng, S. Benson, C. Adam, L. Maierhofer, K. Kozoriz, J.-S. Lee, A. Unciti-Broceta, M. Vendrell, *Nat. Commun.* **2024**, *15*, 7689.

[6] a) M. I. Sanchez, C. Penas, M. E. Vazquez, J. L. Mascarenas, *Chem. Sci.* **2014**, *5*, 1901-1907; b) T. Volker, F. Dempwolff, P. L. Graumann, E. Meggers, *Angew. Chem. Int. Ed.* **2014**, *53*, 10536-10540; c) C. Vidal, M. Tomás-Gamasa, P. Destito, F. López, J. L. Mascareñas, *Nat. Commun.* **2018**, *9*, 1913; d) Y. Okamoto, R. Kojima, F. Schwizer, E. Bartolami, T. Heinisch, S. Matile, M. Fussenegger, T. Ward, *Nat. Commun.* **2018**, *9*, 1943; e) C. Vidal, M. Tomás-Gamasa, A. Gutiérrez-González, J. L. Mascareñas, *J. Am. Chem. Soc.* **2019**, *141*, 5125-5129; f) V. Sabatino, J. G. Rebelein, T. R. Ward, *J. Am. Chem. Soc.* **2019**, *141*, 17048-17052; g) S. Eda, I. Nasibullin, K. Vong, N. Kudo, M. Yoshida, A. Kurbangalieva, K. Tanaka, *Nat. Catal.* **2019**, *2*, 780– 792.

[7] a) K. Tsubokura, K. K. H. Vong, A. R. Pradipta, A. Ogura, S. Urano, T. Tahara, S. Nozaki, H. Onoe, Y. Nakao, R. Sibgatullina, A. Kurbangalieva, Y. Watanabe, K. Tanaka, *Angew. Chem. Int. Ed.* **2017**, *56*, 3579-3584; b) A. M. Perez-Lopez, B. Rubio-Ruiz, V. Sebastian, L. Hamilton, C. Adam, T. L. Bray, S. Irusta, P. M. Brennan, G. C. Lloyd-Jones, D. Sieger, J. Santamaria, A. Unciti-Broceta, *Angew. Chem. Int. Ed.* **2017**, *56*, 12548-12552; c) K. Vong, T. Yamamoto, T. C. Chang, K. Tanaka, *Chem. Sci* **2020**, *11*, 10933-10938; d) M. C. Ortega-Liebana, N. J. Porter, C. Adam, T. Valero, L. Hamilton, D. Sieger, C. G. Becker, A. Unciti-Broceta, *Angewandte Chemie-International Edition* **2022**, *61*, e202111461..

[8] a) R. Cao-Milan, S. Gopalakrishnan, L. D. He, R. Huang, L. S. Wang, L. Castellanos, D. C. Luther, R. F. Landis, J. M. V. Makabenta, C. H. Li, X. Z. Zhang, F. Scaletti, R. W. Vachet, V. M. Rotello, *Chem* **2020**, *6*, 1113-1124; b) S. Fedeli, R. Huang, Y. Oz, X. Zhang, A. Gupta, S. Gopalakrishnan, J. M. V. Makabenta, S. Lamkin, A. Sanyal, Y. Xu, V. M. Rotello, *ACS Appl. Mater. Inter.* **2023**, *15*, 15260-15268.

[9] a) Y. Bai, X. Feng, H. Xing, Y. Xu, B. K. Kim, N. Baig, T. Zhou, A. A. Gewirth, Y. Lu, E. Oldfield, S. C. Zimmerman, *J. Am. Chem. Soc.* **2016**, 138, 11077-11080; b) J. Clavadetscher, S. Hoffmann, A. Lilienkampf, L. Mackay, R. M. Yusop, S. A. Rider, J. J. Mullins, M. Bradley, *Angewandte Chemie-International Edition* **2016**, *55*, 15662-15666; c) Y. L. Liu, S. Pujals, P. J. M. Stals, T. Paulohrl, S. I. Presolski, E. W. Meijer, L. Albertazzi, A. R. A. Palmans, *J. Am. Chem. Soc.* **2018**, *140*, 3423-3433; d) J. Miguel-Ávila, M. Tomás-Gamasa, A. Olmos, P. J. Pérez, J. L. Mascareñas, *Chem. Sci.* **2018**, *9*, 1947-1952; e) F. M. Wang, Y. Zhang, Z. W. Liu, Z. Du, L. Zhang, J. S. Ren, X. Qu, *Angew. Chemie Int. Ed.* **2019**, *58*, 6987-6992; f) X. Wang, Y. J. Liu, X. Y. Fan, J. Wang, W. S. C. Ngai, H. Zhang, J. F. Li, G. Zhang, J. Lin, P. R. Chen, *J. Am. Chem. Soc.* **2019**, *141*, 17133; g) M. van de L'Isle, S. Croke, T. Valero, A. Unciti-Broceta, *Chem. Eur. J.* **2024**, *30*, e202400611.

[10] a) M. A. Miller, B. Askevold, H. Mikula, R. H. Kohler, D. Pirovich, R. Weissleder, *Nat. Commun.* **2017**, *8*, 15906; b) M. Hoop, A. S. Ribeiro, D. Rösch, P. Weinand, N. Mendes, F. Mushtaq, X.-Z. Chen, Y. Shen, C. F. Pujante, J. Puigmartí-Luis, J. Paredes, B. J. Nelson, A. P. Pêgo, S. Pané, *Adv. Funct. Mater.* **2018**, *28*, 1705920; c) Z. Du, C. Liu, H. L. Song, P. Scott, Z. Q. Liu, J. S. Ren, X. G. Qu, *Chem* **2020**, *6*, 2060-2072; d) Z. Chen, H. Li, Y. Bian, Z. Wang, G. Chen, X. Zhang, Y. Miao, D. Wen, J. Wang, G. Wan, Y. Zeng, P. Abdou, J. Fang, S. Li, C.-J. Sun, Z. Gu, *Nat. Nanotech.* **2021**, *16*, 933-941; e) C. Adam, T. L. Bray, A. M. Perez-Lopez, E. H. Tan, B. Rubio-Ruiz, D. J. Baillache, D. R. Houston, M. J. Salji, H. Y. Leung, A. Unciti-Broceta, *J. Med. Chem.* **2022**, *65*, 552-561.

[11] a) B. Rubio-Ruiz, A. M. Perez-Lopez, L. Uson, M. C. Ortega-Liebana, T. Valero, M. Arruebo, J. L. Hueso, V. Sebastian, J. Santamaria, A. Unciti-Broceta, *Nano Lett.* **2023**, *23*, 804-811; b) L. Deng, A. Sathyan, C. Adam, A. Unciti-Broceta, V. Sebastian, A. R. A. Palmans, *Nano Lett.* **2024**, 24, 7, 2242–2249.

[12] a) L. Oliveira, B. J. Stenton, V. B. Unnikrishnan, C. R. D. Almeida, J. Conde, M. Negro, F. S. S. Schneider, C. Cordeiro, M. G. Ferreira, G. F. Caramori, J. B. Domingos, R. Fior, G. J. L. Bernardes, *J. Am. Chem. Soc.* 2020, **142**, 10869; b) T. Sun, T. Lv, J. Wu, M. Zhu, Y. Fei, J. Zhu, Y. Zhang, Z. Huang, *J. Med. Chem.* **2020**, *63*, 13899-13912.

[13] C. Zhang, C. Xu, X. Gao, Q. Yao, *Theranostics* **2022**, *12*, 2115–2132.

[14] a) J. I. Garcia-Peiro, J. Bonet-Aleta, J. Santamaria, J. L. Hueso, *Chem. Soc. Rev.* **2022,** *51*, 7662-7681; b) D. Pedone, M. Moglianetti, E. De Luca, G. Bardi, P. P. Pompa, *Chem. Soc. Rev.* **2017**, *46*, 4951-4975.

[15] a) W. Li, Z. Sun, D. Tian, I. P. Nevirkovets, S. X. Dou, *J. Appl. Phys.* **2014**, *116*, 33911; b) K. Shim, J. Kim, Y.-U. Heo, B. Jiang, C. Li, M. Shahabuddin, K. C.-W. Wu, M. S. A. Hossain, Y. Yamauchi, J. H. Kim, *Chem. Asian J.* **2017**, 12, 21-26; c) J. I. Garcia-Peiro, J. Bonet-Aleta, M. L. Tamayo-Fraile, J. Santamaria, J. L. Hueso, *Nanoscale*, **2023**, *15*, 14399-14408.

[16] Z. Qing, G. Luo, S. Xing, Z. Zou, Y Lei, J. Liu, R. Yang, *Angew. Chemie Int. Ed.* **2020**, *132*, 14148-14152.

[17] C. Adam, A. M. Pérez-López, L. Hamilton, B. Rubio-Ruiz, D. Sieger, P. M. Brennan, A. Unciti-Broceta. *Chem. Eur. J.* **2018**, *24*, 16783-16790.

[18] J. P. Armand, M. Ducreux, M. Mahjoubi, D. Abigerges, R. Bugat, G. Chabot, P. Herait, M. de Forni, P. Rougier, *Eur. J. Cancer*, **1995**, *31*, 1283-1287.

[19] M. De Pascale, L. Bissegger, C. Tarantelli, F. Beaufils, A. Prescimone, H. M. S. Hedad, O. Kayali, C. Orbegozo, L. Raguž, T. Schaefer, P. Hebeisen, F. Bertoni, M. P. Wymann, C. Borsari, *Eur. J. Med. Chem.* **2023**, *248*, 115038.

[20] P. Letrado, I. de Miguel, I. Lamberto, R. Díez-Martínez, J. Oyarzabal, *Cancer Res.* **2018**, *78*, 6048-6058.

10.1002/anie.202424037

RESEARCH ARTICLE

Entry for the Table of Contents

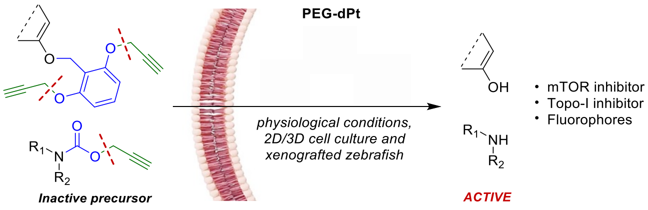

Bioorthogonal platinum chemistry! Dendritic Pt nanoparticles shielded by Pt-S PEGylation demonstrated high biocompatibility and the capacity to mediate uncaging reactions in cancer cells, enabling the *in situ* release of anticancer drugs in 2D and 3D culture, and *in vivo*.

Institute and/or researcher Twitter usernames: @boomchemistry; @INMAdivulga